Irrig Drainage Syst (2007) 21:197–218
DOI 10.1007/s10795-007-9029-z

Mapping and assessing water use in a Central Asian irrigation system by utilizing MODIS remote sensing products

Christopher Conrad · Stefan W. Dech · Mohsin Hafeez · John Lamers · Christopher Martius · Günter Strunz

Published online: 13 July 2007

Abstract Spatial and temporal patterns of water depletion in the irrigated land of Khorezm, a region located in Central Asia in the lower floodplains of the Amu Darya River, were mapped and monitored by means of MODIS land products. Land cover and land use were classified by using a recursive partitioning and regression tree with 250 m MODIS Normalized Difference Vegetation Index (NDVI) time series. Seasonal actual evapotranspiration (ET_{act}) was obtained by applying the Surface Energy Balance Algorithm for Land (SEBAL) to 1 km daily MODIS data. Elements of the SEBAL based METRIC model (Mapping Evapotranspiration at high Resolution and with Internalized Calibration) were adopted and modified. The upstream–downstream difference in irrigation was reflected by analyzing agricultural land use and amounts of depleted water (ET_{act}) using Geographical Information Systems (GIS). The validity of the MODIS albedo and emissivity used for modeling ET_{act} was assessed with data extracted from literature. The r^2 value of 0.6 indicated a moderate but significant association between ET_{act} and class-A-pan evaporation. Deviations of ET_{act} from the 10-day reference evapotranspiration of wheat and cotton were found to be explainable. In Khorezm, seasonal maximum values superior to 1,200 and 1,000 mm ET_{act} were estimated for rice and cotton fields, respectively. Spatio-temporal

C. Conrad (✉) · S. W. Dech
Remote Sensing Unit, Department of Geography, University of Wuerzburg,
Am Hubland, 97074 Wuerzburg, Germany
e-mail: christopher.conrad@mail.uni-wuerzburg.de

C. Conrad · S. W. Dech · G. Strunz
German Aerospace Center (DLR)–German Remote Sensing Data Center (DFD),
Oberpfaffenhofen, 82234 Wessling, Germany

M. Hafeez
Land and Water Division, Commonwealth Scientific & Industrial Research Organization, CSIRO,
Locked Mail Bag 588, Wagga Wagga NSW 2678, Australia

J. Lamers · C. Martius
Center for Development Research (ZEF),
Walter-Flex-Strasse 3, 53113 Bonn, Germany

comparisons of agricultural land use with seasonal ET_{act} disclosed unequal water consumption in Khorezm. Seasonal ET_{act} on agricultural land decreased with increasing distance to the water intake points of the irrigation system (972–712 mm). Free MODIS data provided reliable, exhaustive, and consistent information on water use relevant for decision support in Central Asian water management.

Keywords Central Asia · MODIS · Time series · Seasonal actual evapotranspiration · Spatially distributed modeling

Introduction

Water mismanagement, pollution, rapid population growth, and water-related environmental and ecological problems are major issues in the Aral Sea basin, located in the semiarid and desert areas of Central Asia (Martius et al. 2004). Although these parts of the desert regions of Central Asia are associated with high evaporation and infiltration rates, the main reason for the shrinking of the Aral Sea (Ressl and Micklin 2004) and the resulting 'Aral Sea Syndrome' (WBGU 1998) is the human-induced diversion of river water for irrigated agriculture. Between 1960 and 1990, cotton cultivation in Central Asia expanded from 3 million ha to 8 million ha (Micklin 1991). Since independence from the Soviet Union in 1992, Uzbekistan has continued the cotton production practices developed under the Soviet planned economy and in addition introduced a state order for winter wheat from 1995 onwards (Ruzmetov et al. 2003). Presently, Uzbekistan and the other central Asian countries top the list of highest per-capita water use (WWF 2002).

Due to the aridity of the climate, agricultural production on more than 90% of the arable land in Uzbekistan is only feasible with irrigation (Chub 2000). The agriculture-based economy of the Khorezm region in northwest Uzbekistan highly depends on irrigation from the Amu Darya River. The development of extensive irrigation schemes but with improperly working drainage systems caused rising groundwater tables, and consequently drastically changed the local and regional hydrology (Ibrakhimov 2005). In addition, the irrigation water-use efficiency is very low (Dukhovny et al. 2004) and there is an urgent need to find options to "grow more crop per drop."

One important means to approach this goal may be to increase the low water use efficiencies, which is feasible when management decisions are based on an analysis of accurate hydrological information at each scale. Unfortunately, until today water resource managers in Central Asia face both a paucity of reliable and consistent information (Dukhovny et al. 2004) and inadequate and inappropriate tools for analysis, especially at the irrigation system and watershed level (Chemin et al. 2004). The use of appropriate, reliable, and consistent information at the irrigation system level can improve water management significantly, e.g., by indicating necessary changes for managing water more beneficially, negative impacts in downstream areas can be minimized. An important challenge for water managers is, furthermore, obtaining timely, objective and accurate information on water usage at each spatial scale. Despite existing land and water regulations from field to basin scale, major problems in the Central Asia countries remain the inconsistent and incomplete information about the actual resource usage (Chemin et al. 2004) and the absence of monitoring or control facilities (Dukhovny et al. 2004). To bridge this gap, spatial and temporal information about the volume of water consumption for the land use classes in the basin are needed. Recent developments in the remote sensing sciences and their application to

water resources management now allow the provision of accurate spatio-temporal information about land and water use patterns in large basin (Schmugge et al. 2002).

The current research was carried out under the framework of the ZEF/UNESCO project, which addresses among other concerns the assessment of valid and reliable information about availability, distribution and usage of water in Khorezm (Martius et al. 2004). To complement the findings on water use and efficiency on the field level (Forkutsa 2006), analyses of land and water use patterns for all of Khorezm have been initiated but still suffer from insufficient information (Schweitzer et al. 2004; Ruecker et al. 2005). The major objective of this study was to map and assess spatio-temporal water use patterns in the large scale irrigation system of Khorezm by utilizing MODIS remote sensing data and GIS to improve decision making. Additional objectives were (1) mapping and validating accurate land cover and land use based on time series of 8-day, 250 m MODIS MOD09 surface reflectance data and (2) assessing the validity of 1 km MODIS MOD11 land surface temperature (LST) data for mapping seasonal actual evapotranspiration by using SEBAL and METRIC.

Remote sensing for irrigation water management

Remote sensing techniques are highly suitable for classifying regional and global scale land cover, and for delineating irrigated areas (Droogers 2002) or land use patterns in agricultural regions (Thenkabail et al. 2005; Bastiaanssen et al. 2000). Several approaches exist to derive land cover and use classes from different types of remote sensing data (Richards and Xiuping 2005). In particular, high temporal resolution data in combination with multitemporal classification strategies have been found useful for describing the temporal dynamics of seasonal vegetation cover and land use in irrigated areas (Thenkabail et al. 2005).

Until 2000, the only sensor providing daily data with an acceptable spatial resolution of 1 km^2 in an operational mode was the Advanced Very High Resolution Radiometer (AVHRR) on board TIROS-N and NOAA 8-15 (Jensen 2000). Essential improvements were obtained with the MODerate resolution Imaging Spectroradiometer (MODIS) on board the Terra (EOS-AM1) and Aqua (EOS-PM1) platforms launched in 1999 and 2002, respectively (Savtchenko et al. 2004). The high spectral resolution of 36 bands allowed improvements in atmospheric correction, which resulted in the reflectance product (Vermote et al. 1997) as a standardized input parameter of the MODIS land product suite (Justice et al. 1998). MODIS spatial resolutions of 250 m within the red and near infrared spectra and of 500 m in the visible and short wave infrared (five bands) spectra increased the level of detail for classification.

Unsupervised clustering techniques were applied to AVHRR time series of Normalized Difference Vegetation Index (NDVI; Loveland et al. 2000) or filtered data (Viovy 2000) to distinguish land cover classes on a continental scale. The results of a cluster analysis of 42 MODIS 500 m 8-day surface reflectance data sets and a complex set of features describing the location of a class within a feature space were integrated into a decision tree to classify different crop rotations in the Ganges and Indus River basins (Thenkabail et al. 2005). DeFries et al. (1998) applied supervised classification trees to metrics of 8 km AVHRR time series resulting in 57 nodes for 17 global land cover classes. One year of monthly 1 km AVHRR data made it possible to distinguish 12 classes by a cascading two-class hierarchy of classification trees (Hansen et al. 2000). MODIS 500 m reflectance data were combined with other GIS data in "classification and logistic regression" trees to derive land use and predict deforestation in Colombia (Etter et al. 2006). Remote sensing techniques also

proved useful for estimating evaporation when solving the energy balance of thermodynamics fluxes at the earth surface. This approach has gained momentum since 1990 due to the relatively low cost of data collection, which amounts to $0.03/ha for irrigated lands (Sakthivadivel et al. 1999). Various methods for estimating actual evapotranspiration (ET_{act}) have been investigated by combining satellite images and ground meteorological data for large areas (Vidal and Perrier 1989; Choudhury 1994; Granger 1997).

One method for estimating ET_{act} is the Surface Energy Balance Algorithm for Land (SEBAL) developed by Bastiaanssen (1995, 2000) and Bastiaanssen et al. (1998). SEBAL is designed for flat terrain in semiarid regions and is based on the calculation of the latent heat of ET (λET) as a residual from the surface energy balance. In recent years, SEBAL has been widely used to model seasonal ET_{act} by utilizing remote sensing data (Bastiaanssen 2002). METRIC extends SEBAL for mountainous relief and couples it with reference evapotranspiration for alfalfa and was used to predict seasonal ET_{act} based on Landsat data in the USA (Allen et al. 2005). Tasumi et al. (2005) demonstrated the internal calibration of SEBAL and METRIC showing with sensitivity analyses the independence of atmospheric influences on the thermal radiation received at the sensor. Verstraeten et al. (2005) analyzed the suitability of different remote sensing approaches in view of operational estimations of ET from NOAA data over European forests.

SEBAL was applied in more than 15 case studies to all remote sensing sensors receiving thermal information (e.g., Landsat TM and ETM, NOAA, ASTER, MODIS, and Meteosat) and carried out worldwide in different climatic regions (Hafeez and Khan 2006). The accuracy of SEBAL measured on a field scale by lysimeter, scintillometer, Bowen ratio towers, or Eddy correlation fluxes varied between 1 and 33% for instantaneous ET and between 2 and 30% for 10-day ET (Bastiaanssen et al. 2005). At the catchment scale, accuracies were estimated by the water balance, which led to results of less than 11%.

Description of the study area

Research was conducted in the Khorezm region, located in the northwest of Uzbekistan and between 60.05 and 61.39 N and 41.13 and 42.02 E of the Greenwich meridian, approximately 225 km south of the present shores of the Aral Sea. Khorezm is part of the lower Amu Darya River floodplain (Fig. 1, upper right map). Besides the capital Urgench, the region encompasses ten administrative districts. Khorezm encompasses an area of about 5,600 km^2, of which 260,000 ha (2,600 km^2) can be irrigated.

The climate in the Khorezm Region is extremely continental (Chub 2000). Potential evapotranspiration exceeds the annual precipitation of about 100 mm between 14 and 16 times (Glazirin et al. 1999). The mean annual air temperature is approximately 13°C and annually 205 frost-free days are recorded (Glazirin et al. 1999; Chub 2000). The main crops are cotton, winter wheat, rice and alfalfa, but livestock rearing is rapidly gaining importance (Mueller 2006).

The water of the Amu Darya River is distributed through six major inlet water constructions. It is supplied in an extensive, hierarchically constructed network of main, inter-farm and on-farm irrigation channels with a total length of 16,233 km and a drainage network of 7,679 km (Fig. 1, main map). Although pumps are used, water flow is overwhelmingly caused by gravity forces. Khorezm receives annually between 3.5 and 5 km^3 water, of which about 95% is designated for agricultural purposes (Conrad 2006). Water is often led to the fields in open, nonlined channels (Ibrakhimov 2005), and losses from evaporation and groundwater discharge are estimated to be 40% or more (Martius et al. 2004).

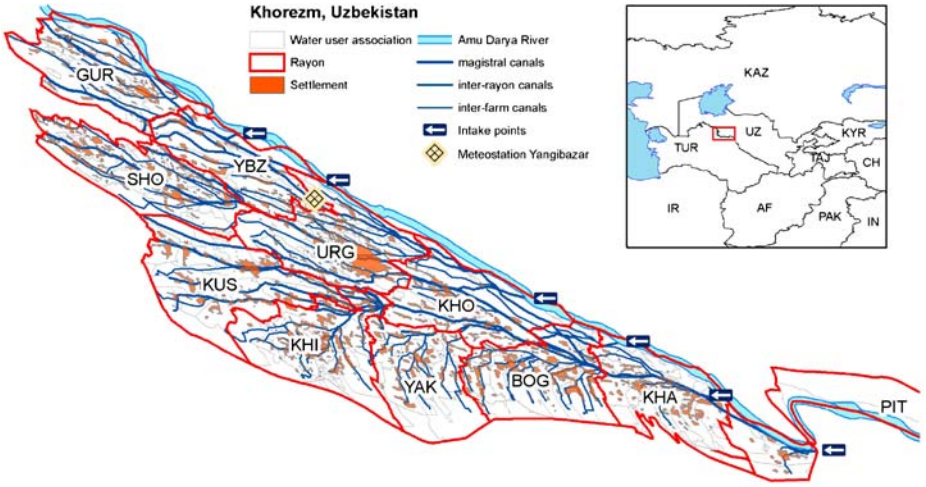

Fig. 1 The irrigation system within the administrative boundaries of Khorezm oblast, Uzbekistan. The small map in the *upper right* corner illustrates the location and dimension of Khorezm within Central Asia

Materials and methods

The study was based on MODIS remote sensing data comprising spectral reflectance (ρ), land surface temperature (LST) and emissivity (ε), surface albedo (α), Normalized Difference Vegetation Index (NDVI), and Leaf Area Index (LAI). Half-hourly measurements of prime meteorological data recorded at a meteorological station within the study area were used to estimate reference evapotranspiration for modelling. After data selection and preprocessing, the methods applied to derive agricultural land use classes and seasonal ET_{act} are specified. Subsequently, a plausibility analysis for the validation of the modeling results is presented, followed by a description of the spatio-temporal analysis using Geographical Information Systems (GIS).

NASA MODIS products

The large MODIS product suite comprises land surface parameters with daily, 8-day, and 16-day temporal resolutions reprojected and gridded in 250, 500 m, and 1 km spatial resolutions (Justice et al. 1998). Overpass LST data necessary for the application of SEBAL (Bastiaanssen et al. 1998) are provided as swath products and needed to be separately pre-processed, which is described below.

Table 1 lists different Terra-MODIS products which were downloaded and preprocessed for the land cover/land use classification and for SEBAL. Detailed information about MOD09 surface reflectance products is provided in Vermote et al. (1997). Wan and Li (1997) describe the retrieval of MOD11 land surface temperature (LST) and emissivity from MODIS data. The algorithms of the vegetation index (MOD13) and the Leaf Area Index (MOD15) products are presented by Huete et al. (2002) and Myneni et al. (2002). The computation of broadband white sky albedo (stored in the MOD43B3 product) by integrating bi-hemispherical reflectance data modeled over MODIS channels 1–7 (0.3–5.0 μm) is explained in Schaaf et al. (2002).

All NASA MODIS land products include so called Quality Assessment Science Data Sets (QA-SDS). Depending on the product, the QA-SDS considers the atmospheric conditions in

Table 1 MODIS data products used to classify land cover/land use and to model seasonal actual evapotranspiration between the 1st of April and the 31st of October 2004 (DOY 92 to DOY 305)

Data product	Layer	Spatial resolution	Temporal resolution	MODIS QA-SDS[a] analysis (quality flags passed)	Linear interpol.
MOD11_L2	LST	1 km[b]	Overpass	General quality: good and acceptable LST	No
	Emissivity	1 km[b]	Overpass	errors up to 4 K accepted	No
	View angle[c]	1 km[b]	Overpass		No
	Recording time	1 km[b]	Overpass		No
MOD13A2	NDVI	1 km	16-day	Usefulness: perfect – good Mixed clouds: no	Yes
MOD15A2	LAI	1 km	8-day	General quality: good and acceptable Cloud state: clear and assumed clear	Yes
MOD43B3	White sky albedo	1 km	16-day	General quality: good and acceptable, Snow: no	Yes
MOD09Q1	Red reflectance	250 m	8-day	General quality: good	Yes
	NIR reflectance			Clouds: clear Band quality: highest	

[a] Quality Assessment Science Data Sets

[b] The swath products were gridded using the MODIS reprojection tool (MRT).

[c] The view angles were analyzed to remove effects from scan geometry caused by increasing IFOV towards the edges of the scan lines.

terms of cloud cover and aerosol content, algorithm choices, processing failures, and error estimations. The software application 'Time Series Generator' (TiSeG, Colditz et al. 2006) was used to exclude invalid data by analyzing the MODIS QA-SDS. With TiSeG, improved time series were built from several gridded MODIS land data products by assessing data quantity against data quality (Conrad et al. 2005). The settings applied are also noted in Table 1. The albedo and the vegetation products NDVI and LAI were interpolated using temporal linear interpolation.

MOD11_L2 LST and emissivity data was preprocessed in three steps. First, the MODIS reprojection tool (MRTSwath) was used to transform the swath data into 1 km grids and for subsetting. Second, the QA-SDS were analysed and all scenes with valid data covering more than 75% of Khorezm were selected (see Fig. 2). This provided 110 overpasses during the 214 day vegetation period from April 1st to October 31st, 2004 for analysis. The third

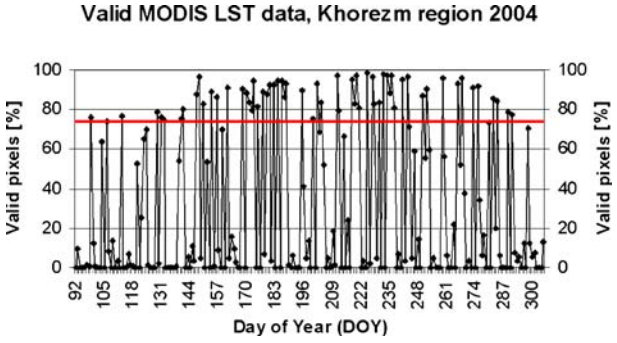

Fig. 2 Daily percentage of valid pixel values for MOD11A1 data 2004 recorded over Khorezm

preprocessing step required sensor related considerations. MODIS is a whisk broom scanner recording one complete scan line after another. Due to the Earth's curvature, the MODIS detector's instantaneous field of view (IFOV) at the edge of the scan lines is 2.0 (4.8) times larger in the track (scan) direction than at nadir (Wolfe et al. 1998). The overlap of the scan lines increases with the scan angle and the same geographic location may be recorded twice. The MRTSwath (L2G approach, see Wolfe et al. 1998) eliminates this "bow-tie effect." However, fitting pixels to a 1 km raster requires the integration of adjacent observations with an increasing error in off-nadir scans, because the IFOV also increases with the scan angle. To minimize this impact, pixels with a view angle higher than 30° off-nadir were removed. At 30° off-nadir view angles, the IFOV is approximately 1.1 km in the along-track and 1.25 km in the across-track direction (Wolfe et al. 1998). In addition, the 75% criteria was applied for each overpass. Finally, 62 MODIS LST observations were considered suitable for analysis of the 214 day vegetation period in 2004. Figure 2 shows the percentage of valid pixels for each day. The red line indicates the limit of 75%, below which the complete overpass was taken out of the further modeling process.

Meteorological data

The application of SEBAL according to the METRIC variant requires several types of meteorological data. Air temperature, relative humidity, wind speed in 2 m height, and net radiation were recorded half-hourly at a meteorological station located in the center of the irrigation system (60°37′12″E, 41°39′10″N; Khamzina 2006). Reference evapotranspiration was obtained by applying the ASCE standardized reference evapotranspiration equation for alfalfa (ET_{rs}; ASCE-EWRI 2005), as suggested by Allen et al (2005). Therefore, coefficients given by ASCE-EWRI were used to estimate ET_{rs} on hourly data, whereas ground heat flux (G) was calculated according to FAO-56 (Allen et al. 1998).

Land cover/land use classification

For classification, temporal signatures of NDVI time series were derived from 46 8-day 250 m surface reflectance data (MOD09Q1, Fig. 3). Mono-modal distributions with one growing peak in the summer characterize cotton and rice (Fig. 3a, b), whereas the winter wheat (Fig. 3c) had its maximum in late spring. The crop rotations of wheat with rice, sunflower, alfalfa, and maize (Fig. 3d) typically showed a bi-modal NDVI development. Non-modal time series represented the land cover classes desert and permanent water surfaces (Fig. 3e, f). Water was spatially stratified into water from lakes and water from river and large channels, because the varying water levels of the rivers generated sudden shifts of the curve above the soil line and resulted in a signature with higher variances than shown by water from lakes. In total, the eleven classes included six nonagricultural surface types ('desert', 'urban settlement', 'rural settlement', 'trees and gardens', 'permanent water surface', and 'rivers and channels') and five agricultural land use types ('cotton', 'rice', 'wheat-fallow', 'wheat-rice', and 'wheat-other').

Up to 60 training and validation samples for each of the eleven classes were extracted from four ASTER scenes acquired on the 17th and 26th of August 2004. They were cross-checked with 120 field samples collected during the summer season of 2004 and with seven observation sites on large homogeneous cotton and rice areas.

For classification, recursive partitioning and regression trees (Breiman et al. 1984) were applied to metrics of MOD09 NDVI time series by employing the statistical open source software R (R Development Core Team 2005). The statistical gini index was used as impurity

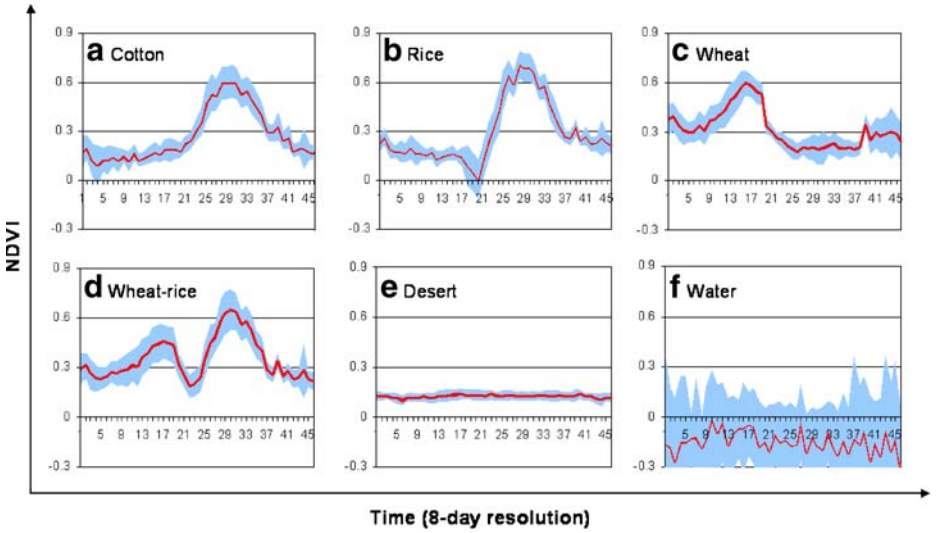

Fig. 3 Temporal NDVI signatures from 8-day 250 m MOD09 surface reflectance data, mean values and standard deviation for cotton (**a**), rice (**b**), wheat (**c**), the crop rotation wheat–rice (**d**), and the land cover classes desert (**e**) and water (**f**)

measure (split criterion); the minimum number within one observation in one node was set to 5 (stop criterion). The method used in this study resembles the approach presented by Hansen et al. (2000).

Applying the classification tree to the training samples led to a misclassification error rate of 3%. Validation samples were used to calculate the overall accuracy and the Kappa coefficient according to Congalton (1991). During post-classification, errors within the settlement pixels were eliminated by using settlement polygons provided by the ZEF/UNESCO GIS Center in Urgench.

Modelling seasonal actual evapotranspiration

Basically, the SEBAL model solves the surface energy balance for each pixel, which results in the latent heat for evapotranspriation (λET). λET is derived by subtracting ground heat fluxes (G) and sensible heat fluxes (H) from the available energy; the net radiation (R_n). MODIS LST, α, ε, and NDVI data were used to calculate R_n and G according to the formulation of SEBAL (Bastiaanssen et al. 1998; Bastiaanssen 2000). The multitemporal approach and the application of SEBAL to large scale MODIS pixels required modifications for the modelling of H (Eq. 1), which is explained in the following.

$$H = \rho_{air} c_p \frac{dT}{r_{ah}} \tag{1}$$

In SEBAL and METRIC (Allen et al. 2005; Tasumi et al. 2005), H usually results from dividing the gradient of vertical temperatures (dT) by the aerodynamic resistance of heat transport (r_{ah}). ρ_{air} is the air density and c_p is the specific heat of air. Atmospheric conditions determine the aerodynamic resistance of heat transport (r_{ah}). Unstable conditions initiate an upward force of air mass; no movement can be registered at neutral conditions, while stable conditions trigger a downward force of air mass. An iterative process integrating the Monin–

Obhukov length to consider the stability of the atmosphere finally results in H (Bastiaanssen et al. 2005).

One basic assumption of SEBAL and METRIC is the linear relationship between dT and land surface temperature (Bastiaanssen et al. 1998; Allen et al. 2005). The linear equation is computed using two anchor points, where H can be calculated by using the surface energy balance. For a completely dry (hot) pixel the latent heat of evaporation is zero. Thus H can be calculated as the difference between R_n and G, immediately resulting in dT_{hot} (Bastiaanssen et al. 1998). Both SEBAL and METRIC characterize hot pixels as nonvegetated dry areas and at best bare soil located close to the meteorological station (Allen et al. 2002). Completely cold pixels such as water surfaces are presumed to consume all available energy for evaporation processes, from which dT_{cold} becomes zero (Bastiaanssen et al. 1998).

In METRIC, well-vegetated fields are selected as cold pixels. H at the cold anchor point (H_{cold}) is expressed as $R_n - G - k \times \lambda ET_{rs}$ where ET_{rs} is the standardized reference evapotranspiration for alfalfa (ASCE-EWRI 2005). The k-factor considers well-watered conditions at the cold pixel which outrange other densely vegetated fields due to higher surface wetness. Allen et al. (2005) assumed k to be 1.05 and included NDVI corrections of k for initial and late growing seasons, when well-watered vegetation pixels are absent.

The selection of homogeneous cold and hot pixels over the whole season by using low spatial resolution remote sensing data sets leads however to uncertainties in heterogeneous landscapes. One square kilometer pixels identified as well-watered vegetation are at least partly covered by roads and houses or smaller irrigation and drainage canals. Spatial variations within the agricultural plots are also possible. Similarly, pure nonvegetated pixels on the 1 km^2 scale are only located in the desert, often far away from the meteorological station, whereas pixels representing nonvegetated land in the irrigated area again often include spots of vegetation, gardens, parts of vegetated fields and at least small or dry irrigation and drainage channels. In this study, a second k-factor for the hot pixel and a slightly finer specification of the k-factor for the cold pixel (Allen et al. 2005) are suggested.

For the hot pixel (Eq. 2) vegetation cover is considered in the case that the NDVI excels the average values of the sandy surface of the surrounding desert (0.15). The factor k_{hot} is defined as a function of NDVI, with k_{hot}=NDVI−0.15 if the NDVI is greater than 0.15, and k_{hot}=0, otherwise.

$$H_{hot} = R_n - G - k_{hot}(NDVI)^{*}\lambda ET_{ref} \tag{2}$$

METRIC uses a soil water balance to account for possible effects of antecedent precipitation at the hot anchor point, which is not reflected by the NDVI. However, in the vegetation period 2004 total precipitation only reached 48 mm. Consequently, influences of soil moisture were assumed to be negligible. In addition, the introduced automated selection process of the anchor points screened all parts of the investigation area, where the probability to find effectively dry pixels is always high due to the patchiness of precipitation in arid regions. Corrections for soil moisture which are part of METRIC were therefore omitted in this approach due to local weather conditions in Khorezm.

For the computation of H_{cold} at the climax of the vegetation period (NDVI≥0.65) k_{cold} was implemented as 1.05 for the same reasons given by Allen et al. (2005): the probability to find pixels within the 240,000 ha sized irrigated network surpassing other pixels with comparably dense and well watered vegetation due to surface wetness was presumed to be high. Adjustments were applied to k_{cold} using the NDVI to account for low vegetation cover during initial and vegetative crop stages or after harvest (k_{cold}=1.05−(0.65−NDVI)/2). In addition rice, water, and other nonagricultural land cover were expected to be absent at the

cold anchor point on the 250 m subpixel scale. Thus, H_{cold} is a written as function of NDVI and the actual land cover (Eq. 3):

$$H_{cold} = R_n - G - k_{cold}(NDVI, \text{landcover})^{*}\lambda ET_{ref} \quad (3)$$

To apply the model on daily data, automated selection of the hot and the cold pixels was necessary to reduce processing time. The presented automated selection process employed remotely sensed information on vegetation density and water conditions when assessing the pixels. Vegetation density can be biophysically related to the leaf area index (LAI, Huete et al. 2002). The land surface temperature (LST) describes the skin temperature of soil and vegetation cover, on which ET has a cooling effect (Verstraeten et al. 2005). For the automated calculation of ET over European forests using NOAA data, Verstraeten et al. (2005) suggested a combination of NDVI and LST as an indication of the vegetation cover and water conditions of a single pixel. LST and LAI were preferred for selecting the hot and cold pixels by Allen et al. (2002). In the presented approach, low LAI values and high land surface temperature characterize hot pixels; high LAI values describe dense vegetation, which in combination with relatively low surface temperatures indicates high ET values (Table 2).

Additionally, the land cover and land use classification is included. Both pixels should originate from the agricultural area in order to discard lakes, desert or settlement pixels from the analysis. Rice fields were unsuitable for the automation process, firstly because they are initially completely covered with water while METRIC requires vegetated areas, and secondly because the literature on the later growing stages gives inconsistent values for the actual water consumption of rice fields (see Mohan and Arumugam 1994).

Table 3 depicts the bi-monthly result of the automated selection process for each of the two model computations. Here, NDVI and LST reflect the introduced k-factors at the cold and hot anchor points. Due to the lack of well watered conditions and the absence of full vegetation cover within one entire MODIS pixel, k_{cold} of less than 1 were found in the early vegetation period. The increase of k_{hot} demonstrates the difficulty in finding 1 km^2 with completely dry conditions in Khorezm during the cotton season, which made adjustments necessary.

Finally, λET transformed to daily ET_{act} by using ET_{ref} as suggested by Tasumi et al. (2005) resulted in amounts of seasonal ET_{act}. The relation ET_{act}/ET_{ref} was interpolated linearly to close gaps caused by missing data. Accordingly, the data gaps in single overpasses resulting from omitting invalid MOD11_L2 data could be filled, except for minor errors owing to the scan angles, as mentioned before.

Table 2 Suggested rules to automate the selection of cold and hot pixels

Cold pixel		Hot pixel	
Verbal formulation	Computation rule	Verbal formulation	Computation rule
Agricultural area	Select from land use classes	Agricultural area	Select from land use classes
No water surface	Actual land use ≠ 'rice', actual land cover ≠ 'water'		
High green vegetation density	Maximum (LAI)	Low green vegetation density	Actual land use≠'fallow' minimum (LAI)
Assumed high evapotranspiration	Minimum (LST)	Assumed low evapotranspiration	Maximum (LST)

Table 3 Environmental situation at the anchor points automatically selected from remote sensing data and resulting *k*-factors for each two computations of SEBAL per month

Date	Cold anchor pixel			Hot anchor pixel		
	LST	NDVI	k_{cold}	LST	NDVI	k_{hot}
08.04.2004	294.88	0.36	0.90	301.18	0.20	0.05
22.04.2004	294.30	0.39	0.92	299.10	0.20	0.05
08.05.2004	306.38	0.43	0.94	310.68	0.21	0.06
20.05.2004	307.20	0.52	0.98	313.42	0.20	0.05
09.06.2004	307.34	0.40	0.93	317.80	0.17	0.02
20.06.2004	309.62	0.36	0.91	320.92	0.20	0.05
06.07.2004	305.36	0.35	0.90	314.64	0.31	0.16
20.07.2004	305.54	0.46	0.95	315.96	0.23	0.08
08.08.2004	302.56	0.62	1.04	309.64	0.29	0.14
21.08.2004	304.24	0.64	1.04	312.28	0.34	0.19
08.09.2004	297.86	0.74	1.05	302.82	0.43	0.28
22.09.2004	298.44	0.63	1.04	304.22	0.36	0.21
08.10.2004	292.26	0.49	0.97	297.34	0.33	0.18
17.10.2004	289.78	0.56	1.01	293.22	0.24	0.09

Validation of ET_{act}

Due to absent lysimeters (Tasumi et al. 2005), scintillometers, Bowen ratio towers, or eddy covariance systems (Bastiaanssen et al. 2005) often used for validation, a stepwise plausibility analysis was carried out to validate the SEBAL modeling results. To account for possible errors caused when using MODIS data, in a first step, albedo and emissivity were compared with the biophysical values of cotton, rice and wheat taken from secondary sources. Secondly, class-A pan evaporation (E_{pan}) was measured in close vicinity of the meteorological station in central Khorezm, which allowed comparison with ET_{act} over water surfaces. The land use classification was used to obtain pixels from water surfaces within a 15 km circle around the location of the class-A pan (9 pixels). In a third step, ET_{act} over vegetated areas was opposed to crop-specific reference evapotranspiration (ET_{crop}) calculated as follows:

$$ET_{crop} = K_c{}^{*}ET_{OS}$$

Crop coefficients (K_c) and the cropping calendar of wheat and cotton for the Khorezm region were obtained from the Central Asian Scientific Research Institute of Irrigation (SANIIRI; Table 4). ASCE standardized reference evapotranspiration for small crops (ET_{os}) similar to grass with an approximate height of 0.12 m was computed from daily meteorological data (ASCE-EWRI 2005). This formula for reference evaporation is equal to that presented in FAO-56 (Allen et al. 1998) and therefore valid for the correct derivation of ET_{crop} according to the FAO manual. The comparisons were made for each 10-day period.

Practical application: spatio-temporal GIS analysis

Water use patterns in Khorezm were analysed in two steps. First, agricultural land use was compared with agricultural water consumption (ET_{act}) to investigate seasonal variations in water distribution. Second, the inventory of agricultural land use and ET_{act} for the Water User Associations (WUAs) was related to their absolute distance to the intake points of the

Table 4 Growing stages and crop coefficients of winter wheat and cotton for the Khorezm region

Crop	Duration of growing stage (days)				Crop coefficients		
	Initial stage	Crop development	Mid-season	Late-season	Initial stage	Mid-season	Late-season
Winter wheat	20	185	30	25	0.3	1.15	0.25
Cotton	60	50	60	55	0.35	1.2	0.7

Source: Oral communication with SANIIRI, Tashkent.

irrigation system to assess upstream–downstream trends in water distribution. For the latter, pixels covering more than 75% agricultural land were included.

To analyze ET_{act} on the MODIS 1 km scale, the 250 m pixels assigned to agricultural land use (cotton, rice, and wheat rotations) were counted within each 1 km^2 pixel [=agricultural land use density (%)]. According to the cropping calendar (see Table 4) five configurations of agricultural land use density were extracted (Table 5). Until the first half of April, the only crop is winter wheat; from the middle of April, cotton is seeded, and rice growing usually starts from mid-May onwards. Wheat harvest occurs from the beginning of June, whereas rice is usually harvested by the end of September. Thus, cotton is the only crop remaining until the end of October.

The GIS data used to calculate the upstream–downstream situation included the irrigation canal network of Khorezm, the Amu Darya River, and the administrative boundaries of the Water User Associations (WUAs). Intersections with the canal system were applied to identify the intake points of the WUA subsystem boundaries. The heads of those parts of the Khorezm irrigation system close to the Amu Darya River were digitized manually. Then, the reticular distance between each Khorezm system intake location and each WUA distribution point was calculated. The distances were averaged for WUAs having more than one subsystem intake point.

Results and discussion

Land cover and land use classification

For the validation of the land cover and land use classification, at best 30 homogeneously covered MODIS pixels were extracted visually for each class from high resolution ASTER data as validation samples. The overall accuracy was 89% and the Kappa coefficient, 0.88. Incorporating inhomogeneous pixels (dominated by more than one class) into the assessment decreased these accuracy indicators.

Table 5 Relevant configuration changes in detectable land use classes during the 2004 vegetation period

Period	Fallow	Wheat	Cotton	Other	Rice
April 1st–April 15th	X	X			
April 16th–May 15th	X	X	X		
May 16th–June 15th		X	X	X	X
June 16th–September 30th	X		X	X	X
October 1st–October 31st	X		X	X	X

The classification results (Fig. 4) showed a clear view of distribution and patterns of actual land use in Khorezm. About 49% of the study area was classified as irrigated land (IL). Agricultural land expansion is mainly delineated by the desert and settlements. As expected, the dominating agricultural crops were cotton (124,000 ha, ~54% of IL) and rice (73,500 ha, ~32% of IL), particularly found in the vicinity of the Amu Darya River. Rice fields covered large parts of the northern rayon Gurlen (see GUR, Fig. 1), which historically is known for rice cultivation. The homogeneity of the agricultural landscape decreased with distance to the river. Concurrently, an increase in crop rotation with winter wheat was identified (54,899 ha, ~24% of IL). Trees and gardens were scattered throughout the entire oblast. Even though settlements could be extracted from the GIS layer, the classes 'rural' and 'urban settlements' indicate a relation between green and impervious portions within a pixel.

Detailed GIS analysis of the classification results allows a comprehensive discussion, which is presented below, including spatio-temporal patterns of water consumption (ET_{act}). The following estimations of ET_{act} are based on these results of the land use classification.

Mapping seasonal actual evapotranspiration (ET_{act})

Comparisons with biophysical values for wheat, cotton, and rice taken from secondary sources indicated the validity of the input parameters albedo and emissivity (Table 6). Averaged MODIS emissivities overestimated the values found in literature, while in general 0.97 is suggested for modeling emissivity of nonmetal surfaces (Campbell and Norman 1998). However, simulations showed that overestimations in emissivity of 0.01 increased the available energy budget at the earth surface by less than 1%.

The r^2 value of 0.6 (n=52 applications of SEBAL) indicated a moderate but significant correlation between ET_{act} over water surfaces averaged for each overpass and daily measured E_{pan}. The resulting trend (E_{pan}=1.04 ET_{act}) showed smaller ET_{act} than E_{pan} because in contrast to the class-A pan, radiation deeply penetrates a natural water body, which makes less energy available for evaporation. Even though physical conditions of evaporation differ widely between water bodies and agricultural crops and SEBAL was

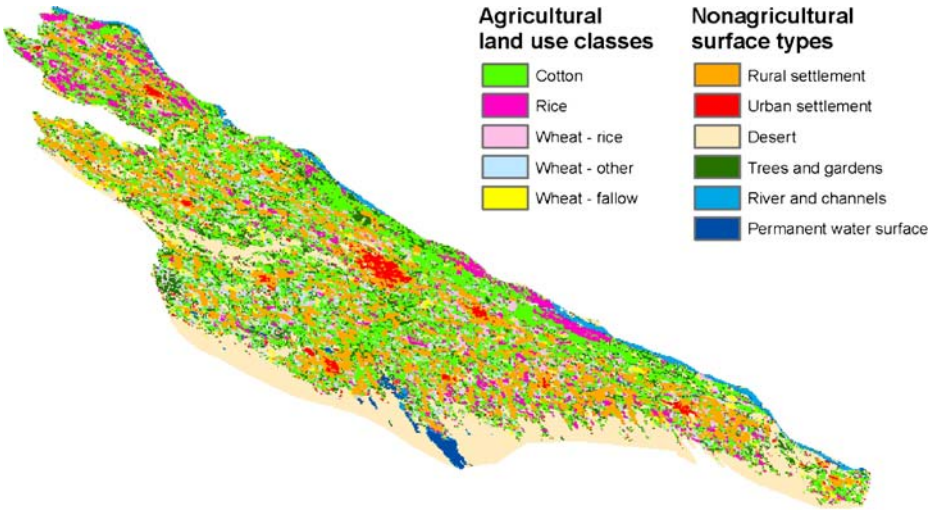

Fig. 4 Spatially distributed land cover and agricultural land use in Khorezm 2004

designed for land rather than for water surfaces, the correlation between ET_{act} and E_{pan} indicates that the model output is plausible.

ET_{crop} was calculated for winter wheat and cotton to compare ET_{act} over the irrigated land of Khorezm. ET_{crop} and ET_{act} summarized for each 10-day periods and standard deviations of ET_{act} are depicted in Fig. 5.

In early April, 10-day ET_{act} overestimated ET_{crop} for winter wheat between 3% and 11%. Underestimations between 18% and 32% were found during the ripening stage (Fig. 5a). The 105% deviation of ET_{act} from ET_{crop} in the wheat harvest stage can be explained by initial leaching and initial growth stages of a second crop (on the sub-pixel level). When excluding the last 10-day period, the coefficient of variation (CV) of ET_{act} ranged between 15 and 21%.

In the initial cotton phase, ET_{act} exceeded ET_{crop} by more than 50% (Fig. 5b), most likely due to high soil evaporation after the leaching period, when high groundwater tables were recorded (Ibrakhimov 2005). In the beginning of July, ET_{act} tends to be lower than expected. Forkutsa (2006) explained similar results from field level by inadequate irrigation within the vegetative growing stage of cotton. During the intensive irrigation phases (July until September), ET_{act} virtually equaled ET_{crop}. Late-season leaching for field preparation explains the higher overestimations (68 and 78%) during harvest time, usually starting at the end of September. CV for 10-day ET_{act} varied between 30 and 44% in April and between 12 and 26% throughout the later growing phases.

Figure 6 shows the spatial distribution of total ET_{act} in the period from 1st of April until the 31st of October, including late leaching and the entire vegetation period. ET_{act} was lowest in desert margins and urban settlements (0–300 mm) and increased in agricultural land to over 1,200 mm. As expected, there were high values for the lakes in southern Khorezm, also because of noise in the input data which occurred at the southern border to Turkmenistan. In central Khorezm (Khonka rayon, KHO, Fig. 1) and in the most northern rayon, Gurlen, (GUR, Fig. 1), minimum seasonal ET_{act} was 700 mm. Well watered locations were also detected south of central Khorezm, where a large branch of the irrigation system is feeding a large fish farm with water (Fig. 6).

Table 6 Emissivity, albedo and surface roughness ($z_{0\ m}$) of wheat, cotton, and rice used as input parameters for modeling ET_{act} compared to literature values

	Crop	μ	σ	Literature biophysical values
Emissivity	Wheat	0.980	0.005	0.981–0.986[a]; 0.976[b]
	Cotton	0.981	0.005	0.96 (for cotton leaves)[c]
	Rice	0.980	0.005	0.97–0.85[d]
Albedo	Wheat	0.182	0.014	0.14–0.22[e]; 0.16–0.22[c], 0.16–0.23[f]
	Cotton	0.178	0.010	0.21[f]
	Rice	0.176	0.013	0.17–0.22[e]; 0.25[g], 0.12[f]

[a] Chen and Zhang (1989)

[b] Huband and Montheith (1986)

[c] Campbell and Norman (1998)

[d] Coll et al. (2004)

[e] Allen et al. (2002)

[f] Halstead et al. (1957)

[g] Mohan and Arumugam (1994)

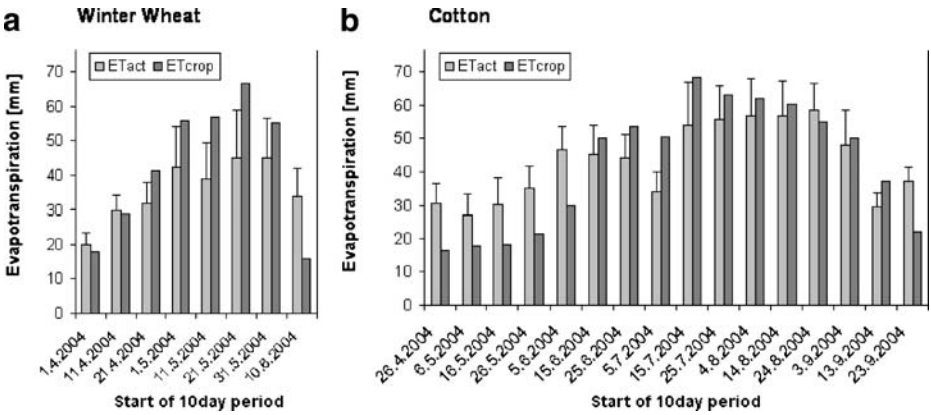

Fig. 5 Comparison between total amounts of ET_{crop} and ET_{act}, for wheat (**a**) and for cotton (**b**)

Crop specific statistics were derived by intersecting the aggregated land cover and land use map with seasonal ET_{act}. Mean values and standard deviations of ET_{act} were 768 and 248 mm on cotton fields, and 798 and 300 mm on rice fields, respectively. On wheat-rice crop rotations, where rice seedlings are commonly transplanted from the nursery to the rice paddies in mid-June, slightly lower average values (739 mm) were modeled.

The results for cotton compare well with the ET_{act} of 706 mm measured in 2004 in an irrigation experiment with furrow-irrigated cotton fields near Tashkent (Ibragimov et al. 2007). Howell et al. (2004) reported an ET_{act} of approximately 750 mm from cotton fields in the arid Texas High Plains.

On rice fields seasonal ET_{act} varies with climatic conditions and vegetation period. In sub-humid India ET_{act} of 596 mm (815 mm) were measured for the 90-day (125-day) period of dry (wet) season rice growth, whereas ET_{os} achieved 470 mm (623 mm; Mohan and Arumugam 1994). Hafeez (2003) reported seasonal ET_{act} of 569 mm (452 mm) for 118 days (130 days) during the dry (wet) season in the Upper Pampanga River Integrated Irrigation System of the Philippines in 2001. In rice growing areas of New South Wales in Australia ET_{act} from 685 to 1,350 mm were measured during the 150 day rice growing season over 32 years (1962–1994), whereas ET_{os} ranged between 960 and 1,412 mm (Humphreys et al. 1994). For rice field in semiarid environments of West Africa, Hendrickx et al. (1986) measured seasonal ET_{act} of 706 mm (443 mm) for a 123 day (92 day) period during two

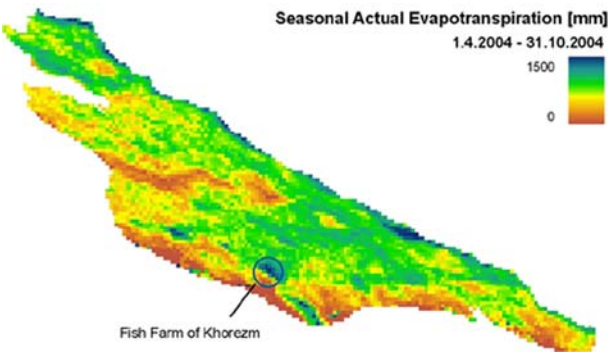

Fig. 6 Seasonal actual evapotranspiration (mm) integrated for parts of the leaching season and covering the whole summer vegetation period in Khorezm 2004

different cropping seasons, whereas ET_{os} was 665 mm (525 mm). The vegetation period for rice in arid Khorezm lasts 135 days.

The assumption of constant weather conditions for the entire irrigation system possibly caused errors especially for the southern parts near the desert. Due to missing reliable meteorological data, the quantification of deviations is yet to be accomplished. In the neighborhood to the desert, ET_{rs} is expected to be higher than in the center of the irrigation system and underestimations of ET_{act} can be a result. On the other hand, this transition zone was assumed to be small because the numerous lakes indicate increased humidity and decreased air temperature also affecting the outer boundaries of the irrigation system. The installation of a small network of meteorological stations could allow these spatial variations to be taken into account.

SEBAL is a worldwide validated model. By selecting MODIS data with scan angles close to nadir the total number of suitable overpasses decreased but potential errors resulting from high IFOV was minimized. In addition, the plausibility analysis confirmed the reliability of the study findings and the comparisons with field experiments also demonstrated the reliability of the presented SEBAL variant. However, for applications in irrigation management in Central Asia, significant optimizations are lacking.

Another relevant aspect for the implementation of this SEBAL variant is the dependence on the actual land use and land cover, which is essential for the selection of the anchor points in the presented approach. Here, reasonable considerations are required to overcome the situation of having a post seasonal land use classification derived from annual time series. Pre-season or early-season land use information would allow intra-seasonal derivations of ET_{act} useful for operational irrigation management.

Spatio-temporal patterns of land and water usage

Multitemporal analysis of the land cover and land use classification result disclosed seasonal variations of water distribution in Khorezm. Figure 7 contrasts the temporal development of agricultural land use density with seasonal ET_{act}. In spring, the homogeneous distribution of winter wheat caused an intermediate land use density throughout the study area, which increased with the seeding of cotton in the last decade of April. The highest density of non-fallow agricultural land occurred between mid-May and mid-June, and decreased slightly after wheat harvest. However, most wheat fields were used to produce a second crop. The map for October showed homogenous cotton distribution in Khorezm.

The ET_{act} map for the first half of April mainly highlights patterns of leaching. Water seemed to be distributed homogeneously over all of Khorezm in the initial cotton growing period, which substantiates the assertion that even in the outer rayons ET_{act} achieve average values. With increasing dominance of rice fields, ET_{act} maps indicated higher water allocations, in particular in the central parts of the irrigation system and in the rice dominated northern irrigation system. Also in the late season, when initial leaching was carried out, the water distribution pattern appeared constant.

Figure 8 summarizes agricultural land use density (a) and ET_{act} on agricultural areas (b) for the entire cropping season resulting from the GIS analysis of the irrigation canal network (Fig. 9). The density of agricultural land within a WUA ranges between 35 and 65% and averages 49%, independent of the location of the WUA within the irrigated area. The low agricultural land use density close to the heads of the irrigation systems was mainly caused by a desert branch reaching deep into the irrigated land. A lower concentration of settlements close to the Amu Darya River explains the peak in the distance class “25–35 km”. Most WUAs within the “45–55 km” distance occur in the surroundings of Urgench (URG,

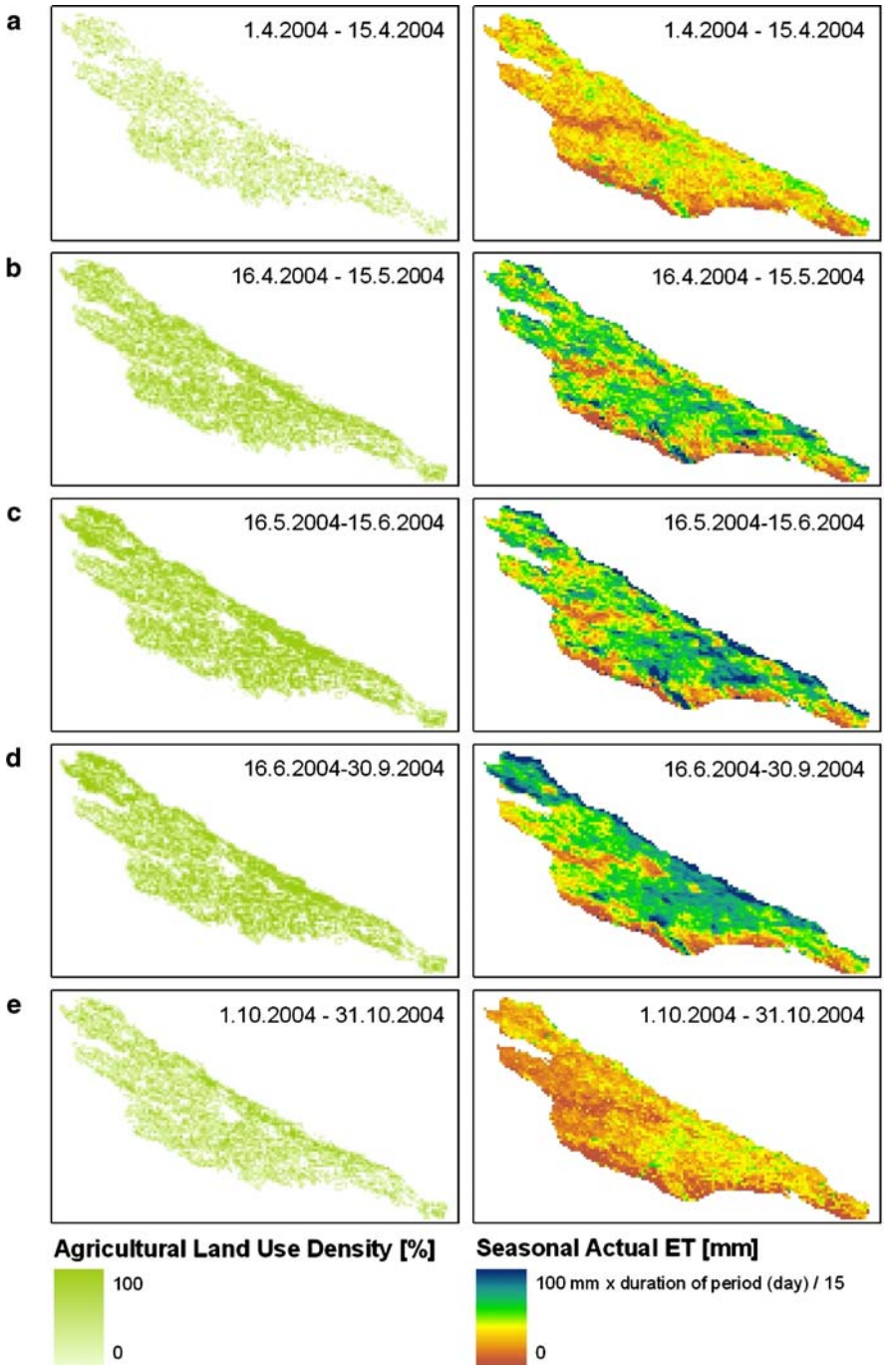

Fig. 7 Actual land use density versus (*left column*) seasonal ET_{act} (*right column*) summarized for the configurations according to the cropping calendar (Table 5). The **a**–**e** opposite these variables for the period from 1.4.2004–15.4.2004, 16.4.2004–15.5.2004, 16.5.2004–15.6.2004, 16.6.2004–30.9.2004, and 1.1.2004–31.10.2004, respectively

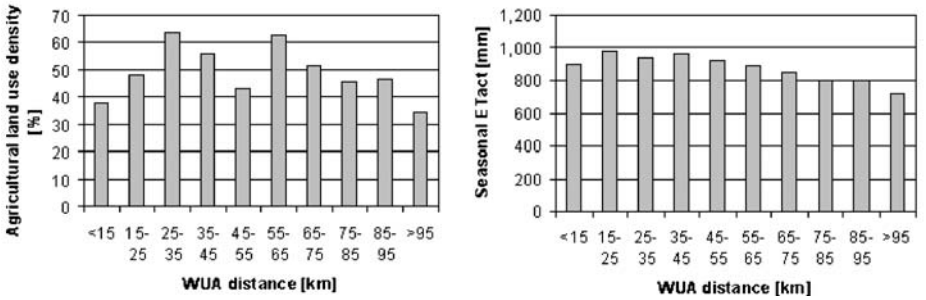

Fig. 8 Relating agricultural land use density and ET_{act} to the reticular distance between WUAs and intake heads within the irrigation system

Fig. 1), which are dominated by settlements. Seasonal ET_{act} used for agriculture indicate a negative upstream–downstream trend of water availability. From class '<15 km' to class '35–45 km' ET_{act} achieved average values between 891 and 975 mm, whereas in the outer reach (class '>95 km') ET_{act} averaged 712 mm.

The classification substantiated the well-known (Mueller 2006), very intensive agricultural use even in regions bordering the desert. The land and water distribution in Khorezm is characterized by high land use density, also in the tail end regions of the irrigation system where low ET_{act} was recorded during the vegetation period. In contrast, high water availability is reported for the downstream parts of the canal network of Khorezm (Mueller 2006; Conrad 2006).

The increase of heterogeneity in crop production in central and downstream Khorezm is evident; the reasons are speculative and may be related to informally driven water allocation and supply strategies, as recently postulated (Wegerich 2004). Intensive crop rotations with winter wheat might be used to optimize income, to fulfill the state order for wheat, to reduce risk, or as a strategy to cope with seasonal droughts. The heterogeneous environmental settings in Khorezm may also be caused by soil texture, and by the level and salinity of groundwater, any of which may provoke large variations in crop water demands.

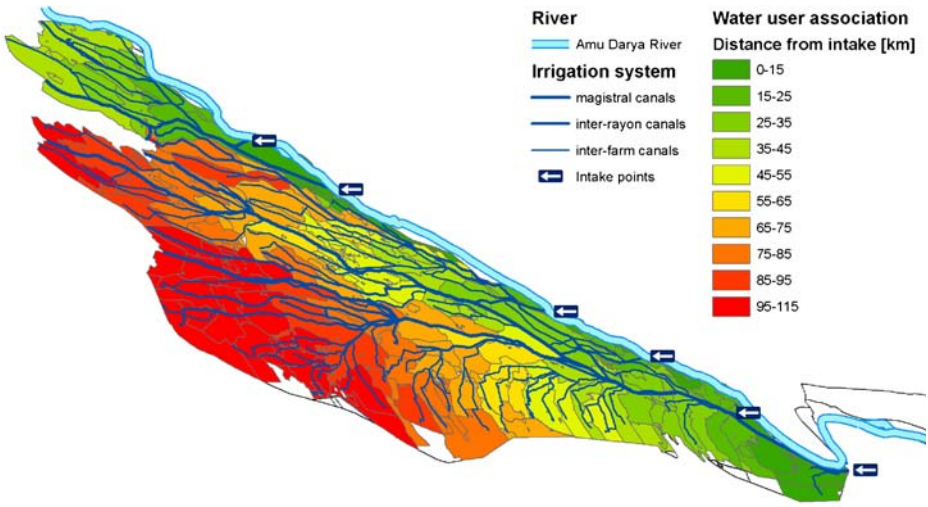

Fig. 9 Average distances (km) between the WUAs and the system intake points of Khorezm

Time series of remotely sensed crop coefficients derived on the field level where the environmental settings are representative and well known, as recently demonstrated by Tasumi and Allen (2007), would make exhaustive and expensive hydrological measurements during the season unnecessary when assessing irrigation performance.

Conclusions

MODIS land products (Justice et al. 1998) provided insights into land and water distribution in Khorezm. Excellent atmospheric conditions in the central Aral Sea basin allowed the generation of nearly gapless time series of remote sensing parameters, especially throughout the vegetation period from April to October. Time series of the 250 m 8-day MODIS MOD09 surface reflectance product contained relevant features to classify and validate all important agricultural land use classes.

Furthermore, modelling ET_{act} became possible for 62 of 214 days between the 1st of April and the 31st of October 2004. Here, extensive preprocessing and pixel selection of 1 km MODIS MOD11_L2 LST/emissivity swath data was necessary to fulfill the requirements of the SEBAL model where overpass records are requested for. As soon as collection 5 of daily MODIS level 3 LST products is available for 2004 (Wan 2007), this time-consuming preparation of level 2 data can be omitted. Interpolation between two overpasses made collection 4 LST data useless for SEBAL in middle and higher latitudes.

The presented results for the Khorezm region show the potential of remote sensing to overcome the lack of reliable, objective, exhaustive, and consistent information on water management issues of Central Asia at a regional scale. With a denser network of meteorological stations permitting better consideration of climatic variations in the irrigation system and in-situ validation facilities for optimizing the model parameterizations, ET_{act} modeled on daily MODIS data and integrated to a monthly product could provide decision support for system-wide operational water management issues.

Acknowledgements This study was funded by the German Ministry of Education and Research (BMBF; project number 0339970C). We are especially grateful to Dr. Gerd Ruecker from the German Aerospace Center (DLR) and Omonbek Salaev from the GIS Center in Urgench, Uzbekistan, for preparing and providing field training samples of land use and essential meteorological and GIS data. We also would like to thank Dr. Tobias Landmann, Department of Geography, University of Wuerzburg, and Susan Giegerich and René Colditz, German Aerospace Center, for their useful comments. The MODIS data used in this study were acquired as part of NASA's Earth Science Enterprise. The algorithms were developed by the MODIS Science Teams. The data were processed by the MODIS Adaptive Processing System (MODAPS) and Goddard Distributed Active Archive Center (DAAC), and are archived and distributed by the Goddard DAAC. We are grateful for the valuable comments from two anonymous reviewers on an earlier version of this manuscript.

References

Allen RG, Pereira LS, Raes D, Smith M (1998) Crop evapotranspiration. Guide-lines for computing crop water requirements. In: FAO irrigation and drainage paper 56, Rome

Allen RG, Waters R, Tasumi M, Trezza R, Bastiaanssen WGM (2002) SEBAL – Surface Energy Balance Algorithm for Land – Idaho implementation – Advanced training and users manual. Idaho, USA

Allen RG, Tasumi M, Morse A, Trezza R (2005) A Landsat-based energy balance and evapotranspiration model in Western US water rights regulation and planning. Irrig Drain Syst 19:251–268

ASCE-EWRI (2005) The ASCE standardized reference evapotranspiration equation. Report by the Task Committee on Standardization of Reference Evapotranspiration, Environmental and Water Resources Institute of the ASCE

Bastiaanssen WGM (1995) Regionalization of surface flux densities and moisture indicators in composite terrain. A remote sensing approach under clear skies in Mediterranean climates. Report 109, Agricultural Research Department, Wageningen, The Netherlands

Bastiaanssen WGM (2000) SEBAL-based sensible and latent heat fluxes in the irrigated Gediz Basin, Turkey. J Hydrol 229:87–100

Bastiaanssen WGM (2002) Satellite surveillance of evaporative depletion across the Indus Basin. Water Resour Res 38(12):1273

Bastiaanssen WGM, Menenti M, Feddes RA, Holtslag AAM (1998) A remote sensing surface energy balance algorithm for land (SEBAL). 1. Formulation. J Hydrol 212–213:198–212

Bastiaanssen WGM, Molden DJ, Makin IW (2000) Remote sensing for irrigated agriculture: examples from research and possible applications. Agric Water Manag 46:137–155

Bastiaanssen WGM, Noordman EJM, Pelgrum H, Davids G, Thoreson BP, Allen RG (2005) SEBAL model with remotely sensed data to improve water-resources management under actual field conditions. J Irrig Drain Eng 131:85–93

Breiman L, Friedman JH, Olshen RA, Stone CJ (1984) Classification and regression trees. CRC Press, New York

Campbell GS, Norman JM (1998) An introduction to environmental biophysics. Springer, Berlin Heidelberg New York

Chemin Y, Platonov A, Ul-Hassan M, Abdullaev I (2004) Water depletion assessment at administrative and irrigation levels. Case Study of Ferghana Province using public remote sensing data. Agric Water Manag 64(3):183–196

Chen J-M, Zhang R-H (1989) Studies on the measurements of crop emissivity and sky temperature. Agric For Meteorol 49:23–34

Choudhury BJ (1994) Synergism of multispectral satellite observations for estimating regional land surface evaporation. Remote Sens Environ 49:264–274

Chub EV (2000) Climate change and its impact on natural resources potential of the republic of Uzbekistan. Tashkent, Uzbekistan, Main Administration on Hydrometeorology under the cabinet of Ministers of the Republic of Uzbekistan. Central Asian Hydrometeorological research institute named after V.A. Bugayev

Colditz RR, Conrad C, Wehrmann T, Schmidt M, Dech S (2006) Generation and assessment of MODIS time series using quality information. In: IEEE International Geoscience and Remote Sensing Symposium, July 31–August 04 2006, Denver, Colorado, USA

Coll C, Valor E, Caselles V, Niclòs R, Rivas, R, Sánchez JM, Galve JM (2004) Evaluation of the Envisat-AATSR land surface temperature algorithm with ground measurements in the Valencia test site. In: Proceedings of the 2004 Envisat & ERS Symposium (ESA SP-572). 6–10 September 2004, Salzburg, Austria

Congalton RG (1991) A review of assessing the accuracy of classifications of remotely sensed data. Remote Sens Environ 37:35–46

Conrad C (2006) Remote sensing based modeling and hydrological measurements to assess the agricultural water use in the Khorezm region (Uzbekistan). PhD Dissertation. University of Wuerzburg (in German)

Conrad C, Colditz RR, Petrocchi A, Ruecker GR, Dech S, Schmidt M (2005) Time-series-generator – a flexible software module to generate and assess time series from NASA MODIS data products. 17. Symposium und Fachmesse für Angewandte Geoinformatik (AGIT). July 6th–8th 2005, Salzburg, Austria (in German)

DeFries RS, Hansen MC, Townshend JRG, Sohlberg RA (1998) Global land cover classifications at 8 km spatial resolution: the use of training data derived from Landsat imagery in decision tree classifiers. Int J Remote Sens 19(16):3141–3168

Droogers P (2002) Global irrigated area mapping: overview and recommendations. Working Paper 36. International Water Management Institute. Colombo, Sri Lanka

Dukhovny VA, Sokolov V, Ziganshima D (2004) Some ideas about IWRM implementation in Central Asia. Seminar on the role of ecosystems as water suppliers. Genava, UNECE

Etter A, McAlpine C, Wilson K, Phinn S, Possingham H (2006) Regional patterns of agricultural land use and deforestation in Colombia. Agric Ecosyst Environ 114:369–386

Forkutsa I (2006) Modeling water and salt dynamics under irrigated cotton with shallow groundwater in the Khorezm region of Uzbekistan. In: Vlek PLG (ed) Ecology and development series 37. Goettingen

Glazirin GE, Shanicheva SC, Shub VE (1999) Brief description of Uzbekistan climate. Tashkent

Granger RJ (1997) Comparison of surface and satellite-derived estimates of evapotranspiration using a feedback algorithm. In: Application of remote sensing in hydrology. Proceedings of the Third International Workshop, NHRI Symposium No. 17, NASA, Goddard Space Flight Center, Greenbelt, MD NHRI, October, 1996

Hafeez MM (2003) Water accounting and productivity at different spatial scales in a rice irrigation system: a remote sensing approach. In: Vlek PLG (ed) Ecology and development series No. 8. Göttingen

Hafeez MM, Khan S (2007) Spatial mapping of actual crop water use in ground water dominant irrigation system. Australian Journal of Agricultural Research (in press)

Halstead MH, Richman RL, Covey W, Merryman JD (1957) A preliminary report on the design of a computer for micrometeorology. J Atmos Sci 14(4):308–325

Hansen MC, DeFries RS, Townshend JRG, Sohlberg RA (2000) Global land cover classification at 1 km spatial resolution using a classification tree approach. Int J Remote Sens 21(6–7):1331–1364

Hendrickx JMH, Vink NH, Fayinke T (1986) Water requirement for irrigated rice in a semi-arid region in West Africa. Agric Water Manag 11(1):75–90

Howell TA, Evett SR, Tolk JA, Schneider AD (2004) Evapotranspiration of full-, deficit-irrigated, and dryland cotton on the Northern Texas High Plains. J Irrig Drain Eng 130(4):277–285

Huband NDS, Monteith JL (1986) Radiative surface temperature and energy balance of a wheat canopy. Part I: comparison of radiative and aerodynamic canopy temperature. Boundary-Layer Meteorol 36:1–17

Huete A, Didan K, Miura T, Rodriguez EP, Gao X, Ferreira LG (2002) Overview of the radiometric and biophysical performance of the MODIS vegetation indices. Remote Sens Environ 83(1–2):195–213

Humphreys E, Meyer WS, Prathapar SA, Smith DJ (1994) Estimation of evapotranspiration from rice in southern New South Wales: a review. Aust J Exp Agric 34(7):1069–1078

Ibrakhimov M (2005) Spatial and temporal dynamics of groundwater table and salinity in Khorezm (Aral Sea Basin), Uzbekistan. Göttingen, Germany

Ibragimov N, Evett SR, Esanbekov Y, Kamilov BS, Mirzaev L, Lamers JPA (2007) Water use efficiency of irrigated cotton in Uzbekistan under drip and furrow irrigation. Agric Water Manag 90:112–120

Jensen JR (2000) Remote sensing of the environment: an earth resource perspective. Prentice Hall, Upper Saddle River, NJ, USA

Justice CO, Vermote EF, Townshend JRG, DeFries RS, Roy DP, Hall DK, Salomonson VV, Privette J, Riggs G, Strahler AH, Lucht W, Myneni R, Knjazihhin Y, Running S, Nemani R, Wan Z, Huete A, van Leeuwen W, Wolfe RE, Giglio L, Muller J-P, Lewis P, Barnsley M (1998) The moderate resolution imaging spectroradiometer (MODIS): land remote sensing for global change research. IEEE Trans Geosci Remote Sens 36:1228–1249

Khamzina A (2006) The assessment of tree species and irrigation techniques for afforestation of degraded agricultural landscapes in Khorezm, Uzbekistan, Aral Sea Basin. In: Vlek PLG (ed) Ecology and development series 39. Goettingen, Germany

Loveland TR, Reed BC, Brown JF, Ohlen DO, Zhu Z, Yang L, Merchant JW (2000) Development of a global land cover characteristics database and IGBP DISCover from 1 km AVHRR data. Int J Remote Sens 21(6–7):1303–1330

Martius C, Lamers JPA, Wehrheim P, Schoeller-Schletter A, Eshchanov R, Tupitsa A, Khamzina A, Akramkhanov A, Vlek PLG (2004) Developing sustainable land and water management for the Aral Sea Basin through an interdisciplinary research. In: Seng V, Craswell E, Fukai S (eds) Water in agriculture, ACIAR Proceedings No. 116 Canberra, Australia

Micklin PP (1991) The water management crisis in Soviet Central Asia. The Carl Beck Papers in Russian and East European Studies. University of Pittsburgh, Pennsylvania, USA

Mohan S, Arumugam N (1994) Irrigation crop coefficients for lowland rice. Irrig Drain Syst 8:159–176

Mueller M (2006) Sectoral and economy-wide effects of different land and water use reforms. University of Bonn, Germany

Myneni RB, Hoffman S, Knyazikhin Y, Privette JL, Glassy J, Tian Y, Wang Y, Song X, Zhang Y, Smith GR, Lotsch A, Friedl M, Morisette JT, Votava P, Nemani RR, Running SW (2002) Global products of vegetation leaf area and fraction absorbed PAR from year one of MODIS data. Remote Sens Environ 83 (1–2):214–231

R Development Core Team (2005) R: a language and environment for statistical computing. R Foundation for Statistical Computing. Vienna, Austria

Ressl R, Micklin PP (2004) Morphological changes in the Aral Sea: satellite imagery and water balance model. In: Nihoul JCJ, Zavialov PO, Micklin PP (eds) Dying and dead seas: climatic versus anthropic causes: proceedings of the NATO Advanced Research Workshop Liège, Belgium, 7–10 May, 2003. Nato Science Series: 4. Earth and Environmental Sciences 36

Richards JA, Xiuping J (2005) Remote sensing digital image analysis. An introduction. Springer, Heidelberg, Germany

Ruecker G, Shi Z, Conrad C, Martius C, Lamers J, Strunz G, Vlek P, Dech S (2005) Site-specific cotton yield estimation by multi-temporal remote sensing data and agro-meteorological model applied to the Khorezm region, Aral Sea Basin. Paper presented in INTAS, International Association for the promotion of co-operation with scientists from the New Independent states of the former Soviet Union. Aral Sea Basin Water and Food Conference – Managing Water and Food Quality and Security in Central Asia, 1–4 September 2005, Almaty, Kazakhstan

Ruzmetov B, Rahimov Z, Rudenko I (2003) Analysis of farmer enterprises and agricultural markets. ZEF Working papers for Sustainable Development in Central Asia. Center for Development Research (ZEF). Bonn, Germany

Sakthivadivel R, Thiruvengadachari S, Amerasinghe U, Bastiaanssen WGM, Molden DJ (1999) Performance evaluation of the Bhakra irrigation system, India, using remote sensing and GIS techniques. Research report 28. International Water Management Institute (IWMI)

Savtchenko A, Ouzounov D, Ahmad S, Acker J, Leptoukh G, Koziana J, Nickless D (2004) Terra and Aqua MODIS products available from NASA GES DAAC. Adv Space Res 34(4):710–714

Schaaf CB, Gao F, Strahler AH, Lucht W, Li XW, Tsang T, Strugnell NC, Zhang XY, Jin YF, Muller JP, Lewis P, Barnsley M, Hobson P, Disney M, Roberts G, Dunderdale M, Doll C, d'Entremont RP, Hu BX, Liang SL, Privette JL, Roy D (2002) First operational BRDF, albedo nadir reflectance products from MODIS. Remote Sens Environ 83:135–148

Schmugge TJ, Kustas WP, Ritchie JC, Jackson TJ, Rango Al (2002) Remote sensing in hydrology. Adv Water Resour 25(8–12):1367–1385

Schweitzer C, Rücker GR, Conrad C, Bendix J, Strunz G, Dech S, Göttingen 2004 (2004) Knowledge-based land use classification combining expert knowledge, GIS, multi-temporal Landsat 7 ETM+ and MODIS time series data in Khorezm, Uzbekistan. Proceedings of 1st Göttingen GIS & Remote Sensing Days. Environmental Studies, Goettingen, Germany

Tasumi M, Allen RG (2007) Satellite-based ET mapping to assess variation in ET with timing of crop development. Agric Water Manag 88(1–3):54–62

Tasumi M, Trezza R, Allen RG, Wright JL (2005) Operational aspects of satellite-based energy balance models for irrigated crops in the semi-arid US. Irrig Drain Syst 19(3–4):355–376

Thenkabail PS, Schull M, Turral H (2005) Ganges and Indus river basin land use/land cover (LULC) and irrigated area mapping using continuous streams of MODIS data. Remote Sens Environ 95:317–341

Vermote EF, El Saleous NZ, Justice CO, Kaufman YJ, Privette J, Remer LC, Tanre D (1997) Atmospheric correction of visible to middle infrared EOS-MODIS data over land surface, background, operational algorithm and validation. J Geophys Res 102(14):17131–17142

Verstraeten WW, Veroustraete F, Feyen J (2005) Estimating evapotranspiration of European forests from NOAA-imagery at satellite overpass time: towards an operational processing chain for integrated optical and thermal sensor data products. Remote Sens Environ 96:256–276

Vidal A, Perrier A (1989) Analysis of a simplified relation used to estimate daily evapotranspiration from satellite thermal IR data. Int J Remote Sens 10(8):1327–1337

Viovy N (2000) Automatic Classification of Time Series (ACTS): a new clustering method for remote sensing time series. Int J Remote Sens 21(6–7):1537–1560

Wan Z (2007) Collection 5 changes in the V5 PGE16. In: NASA Goddard Space Flight Center: MODIS land collection 5 changes. http://landweb.nascom.nasa.gov/cgi-bin/QA_WWW/newPage.cgi?fileName=MODLAND_C005_changes. Cited January 5, 2007

Wan Z, Li Z-L (1997) A physics-based algorithm for retrieving land-surface emissivity and temperature from EOS/MODIS Data. IEEE Trans Geosci Remote Sens 35:980–996

WBGU (1998) Worlds in transition. Ways towards sustainable management of fresh water resources. Springer, Berlin Heidelberg New York

Wegerich K (2004) Informal network utilisation and water distribution in two districts in the Khorezm Province, Uzbekistan. Local Environ 9(4):337–352

Wolfe RE, Roy DP, Vermote EF (1998) MODIS land data storage, gridding, and compositing methodology: level 2 grid. IEEE Trans Geosci Remote Sens 36:1324–1338

WWF (2002) Living planet report. World Wide Fund for Nature